Industrial Crops & Products 242 (2026) 122913

Contents lists available at ScienceDirect

Industrial Crops & Products

journal homepage: www.elsevier.com/locate/indcrop

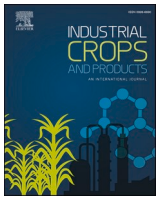

The application of biochar as an alternative to graphite in mineral greases – Tribological and rheological property studies

Monika Łożyńska *, Jarosław Molenda, Rafał Kozdrach, Paweł Radulski, Karolina Dziosa, Monika Makowska

Łukasiewicz Research Network – Institute for Sustainable Technologies, Bioeconomy and Ecoinnovation Centre, 26-600 Radom, Pulaskiego 6/10, Poland

ARTICLE INFO

Keywords:
Biochar
Graphite
Mineral greases
Rheological properties
Tribological properties

ABSTRACT

This study aims to investigate the possibility of replacing a critical raw material - graphite - with an ecological biochar material used as a functional additive to mineral greases thickened with lithium stearate. Biochar is obtained by pyrolysing wheat (*Triticum aestivum*) straw at 500°C in an inert nitrogen atmosphere. To compare the properties of mineral greases including biochar (BW) and graphite (G) additives, six grease compositions were prepared, taking into account the analysis of the effect of carbon additive concentrations (1 %, 3 %, and 5 % BW, and 1 %, 3 %, and 5 % G). Graphite (f < 35 μm) used in commercially available mineral greases serves the purposes of comparative studies. A grease made from a mixture of mineral oils and thickened with lithium stearate is the base grease. No significant changes resulting from replacing graphite with ecological biochar were observed in the rheological tests. The values of the parameters responsible for anti-scuffing properties also suggest that completely replacing graphite with eco-friendly biochar material has no negative effect on these properties of the grease (3 % G - 2617 ± 111 N/mm^2, 3 % BW - 2595 ± 220 N/mm^2). Anti-wear tests reveal the micrometer graphite used has a detrimental effect on surface wear. However, the BW addition raises the wear limit by up to 43 % compared to the base grease. The analysis of the wear traces, along with the determination of surface roughness, demonstrated that the protective mechanism of the biochar-added grease is a consequence of several overlapping processes resulting from the specific properties of biochar.

1. Introduction

The friction and wear of surfaces of mechanical components in contact generate significant energy losses. It is estimated that up to 25 % of global energy is lost to overcoming friction and wear, which in developed economies translates into a loss of several percent of gross domestic product (Holmberg and Erdemir, 2017; Vaziriserehk et al., 2019). To reduce these losses, lubricants are used, materials that create a thin lubricating layer between moving parts, reducing the coefficient of friction and protecting against wear. Lubricants can have a mineral or synthetic base. Mineral greases, made of base oils derived from petroleum, dominate the market due to their low price and easy availability. Numerous chemical additives and solid particles are used to achieve good lubricating properties. The main groups of 2D lubricant additives include graphite (Kumar et al., 2020b; Kumar et al., 2021; Wu et al., 2020) and its derivatives (graphene, graphene oxide (GO), reduced graphene oxide (rGO) (Larsson et al., 2021; Song et al., 2016; Li et al., 2020, Marlinda et al., 2023)) and 1D materials (carbon nanotubes (CNTs) (Zhang et al., 2009)). Their favorable lubricating properties result from their characteristic structure and high mechanical strength. Graphite is an arrangement of parallel layers of carbon atoms that slide one over the other, acting as moving bearings between contacting surfaces (Rahman et al., 2022). Similarly, graphene exhibits very high mechanical strength and extremely high thermal conductivity, which helps reduce friction and wear. Graphene can achieve ultra-low coefficients of friction (so-called superlubrication, COF < 0.01) (Liu et al., 2022). In addition to its layered structure, graphene oxides (GO, rGO) possess numerous functional groups that improve wettability and the ability to form protective layers at interfaces (Wakchaure and Menezes, 2025). Carbon nanotubes (cylindrical windings of graphene sheets) have high strength and conductivity, and thanks to their cylindrical structure, they can act as nano-ball bearings between interfaces (Rahman et al., 2022). Graphene and its derivatives offer excellent tribological properties in laboratory conditions, but their high cost, quality control and

* Corresponding author.
E-mail address: monika.lozynska@itee.lukasiewicz.gov.pl (M. Łożyńska).

https://doi.org/10.1016/j.indcrop.2026.122913
Received 25 September 2025; Received in revised form 12 January 2026; Accepted 11 February 2026
Available online 17 February 2026

dispersion issues, potential interactions with existing additives, regulatory uncertainty, and the lack of a broad performance database make them cautious in the lubricant industry. High-quality single-layer graphene (CVD) is still expensive to mass-produce. However, cheaper methods (liquid exfoliation, GO reduction) produce material of variable quality. Therefore, we are currently seeing more pilot and specialized applications than mass replacement of traditional additives.

Graphite has long been used as a classic EP (extreme-pressure) lubricant additive. Its distinctive lubricating properties result from its layered structure (Kumar et al., 2020b; Kumar et al., 2021; Rahman et al., 2022). Graphite is also characterized by high resistance to oxidation and high temperatures, as well as very good thermal conductivity, which allows for effective removal of friction heat from the surface (Kumar et al., 2020b). However, natural graphite has been recognized by many countries, including the European Union, as a critical and strategic raw material. Currently, over 100,000 tons of graphite are imported into the European Union annually (ECGA, 2022; Regulation of the European Parliament, 2024). Moreover, artificial graphite is much more expensive than natural graphite, which further limits its wide application possibilities.

Biochar, obtained from biomass through pyrolysis, appears to be a promising ecological substitute for graphite in lubricants. It is an amorphous material with a diverse structure, characterized by high porosity and a significant specific surface area. This allows biochar particles to penetrate surface irregularities and form durable protective films. Surface functional groups (hydroxyl, aldehyde, carboxyl) increase biochar's wettability with oil and facilitate adsorption on steel surfaces. Unlike pure graphite, biochar has slightly lower thermal conductivity, but its partial graphite content and porous structure still promote frictional heat dissipation (Guan et al., 2025). It has been proven that the addition of biochar can reduce the coefficient of friction and the wear of friction pairs, improving the performance properties of lubricants (Kozdrach and Radulski, 2025a, 2025b; Molenda et al., 2025b). Another great advantage of biochar is its biodegradability, low production cost, and because it comes from plant waste, it is an easily available material. Agricultural waste is often used for biochar production because it is an easily accessible and low-cost lignocellulosic raw material, which is consistent with the concept of a circular economy. Its use not only reduces the problem of waste biomass overproduction and the associated cost of its disposal but also allows for the production of value-added material (Gotore et al., 2024; Patel and Panwar, 2023). One such product is straw, a crop byproduct remaining in fields after harvesting the main crop. It is primarily used as organic fertilizer, feed, or mulch. Changes in agricultural structure, manifested by a significant decline in livestock farming and an increase in cereal sowing, resulted in an average surplus of 12.5 million tons harvested straw over agricultural use in Poland between 1999 and 2018. Straw harvest significantly exceeds demand, prompting researchers to explore other uses for this type of waste (Gradziuk et al., 2020; Zięta ra and Zieliński, 2018).

The aim of this study is to investigate the possibility of replacing graphite, a critical raw material, with ecological biochar, used as a functional additive in mineral greases thickened with lithium stearate, while maintaining their functional properties. Lubricant compositions with some varying concentrations of carbon additives are tested for their rheological and tribological properties. The criterion is adopted that the introduction of biochar should not degrade the tested lubricant properties compared to the graphite addition.

2. Methodology

2.1. Biomass pyrolysis

Agricultural waste in the form of *T. aestivum* straw is used as the raw material for pyrolysis processes. Based on the authors' previous experience, the following thermal conditions are applied: i) heating to 200°C for 15 min, hold 15 min; ii) heating to 450°C for 30 min, hold 15 min; iii) heating to 500°C for 15 min, hold 15 min (Barszcz et al., 2024; Kaźmierczak et al., 2021; Kozdrach and Radulski, 2025a, Kozdrach and Radulski, 2025b, Makowska and Dziosa, 2024; Molenda et al., 2025b). Pyrolysis is carried out in a nitrogen atmosphere. Drawing on the authors' experience in producing biochar from different lignocellulosic biomasses and in tribology, selecting such pyrolysis parameters is assumed to endow resulting biochar material with properties essential for our aim. Pyrolysis processes were conducted on a laboratory stand equipped with a Czylok FCF-V12RM muffle furnace. The pyrolysis efficiency during biochar production from wheat straw is 26.7 %. The resulting biochar material is ground to obtain a particle size of < 150 μm.

2.2. The characteristics of carbon materials

The elemental composition of the produced biochar is analyzed using a Hitachi SU-70 Scanning Electron Microscope (SEM) with Energy Dispersive Spectroscopy (EDS) microanalyzer. Moisture and ash content are analyzed gravimetrically by heating at 105°C and 815°C, respectively, using a Binder laboratory drying oven and a Thermo Scientific muffle furnace in accordance with the PN-ISO 1171:2002 and ISO 18134 standards. The percentage content is determined based on the mass difference before and after heating. The crystalline structure of the biochar is assessed using Raman spectroscopy with a 532 nm laser excitation wavelength and an exposure time of 60 s. A Jasco NRS 5100 spectrometer is used for the studies. The spectra were recorded in the range from 100 cm^{-1} to 3600 cm^{-1} with a resolution of 3.62 cm^{-1}. Each char is analyzed at 10 measurement points (three repetitions at each point) using the regular grid method. The presence of functional groups on the biochar surface is assessed by FTIR spectra using a Jasco FTIR 6200 spectrometer equipped with a Pike Diamond ATR. A TGS detector serves the analyses in the 4000–650 cm^{-1} range and 4 cm^{-1} resolution. The specific surface area of the biochar is determined by means of the multipoint Brunauer–Emmett–Teller (MBET) method based on N_2 adsorption isotherms (77 K) obtained using an Autosorb IQ analyzer from Quantachrome. Before the analysis, the samples are degassed in vacuum (10^{-7} bar) at 300°C for 12 h.

2.3. Preparation of mineral grease compositions

The base mineral grease (designated MG) is formulated from a mixture of mineral oils (technical cleanliness, Nynas) with a kinematic viscosity of 209.3 ± 2.2 mm^2/s. Lithium stearate (96 %, Roth) serves as a thickener. The mixture is homogenized and heated to 220°C, then cooled to room temperature to solidify the grease. Carbon additives, in the form of powdered biochar and graphite, are added at 1 %, 3 %, and 5 % levels while slowly mixing with a planetary homogenizer for 15 min. The resulting greases are designated as 1 % BW, 3 % BW, and 5 % BW for greases with biochar, and 1 % G, 3 % G, and 5 % G for greases with graphite. This study utilized commercially available graphite with a particle size of < 35 μm, commonly used in commercial graphite mineral lubricants, particularly those intended for the automotive industry. Obtaining fine graphite fractions is, however, expensive, time-consuming, and difficult to achieve on a small scale. The use of biochar with a higher particle size (<150 μm) compared to graphite particles was driven by two factors. First, we aimed to demonstrate that replacing graphite with eco-friendly biochar does not require lengthy grinding to achieve tribological and rheological properties at least similar to those of commercial graphite lubricants. Second, laboratory limitations and difficulties in obtaining such fine material fractions were the goal, thus reducing the cost and time required to prepare biochar materials. To assess the uniformity of carbon additive dispersion within the lubricant matrix, the prepared lubricants are spread on a microscope slide and imaged using a Keyence 3D microscope at 500x optical magnification. To assess particle agglomeration within the lubricant structure, carbon particles are sized at 5 randomly selected points at

1000x magnification.

2.4. Rheological tests

The consistency class of the greases is determined in accordance with the PN-ISO 2137:2021–07 standard. This method involves measuring the depth of gravity immersion of a standardized falling cone for 5 s in the tested grease after 60 kneading cycles. The mechanical stability of the greases is tested in accordance with the PN-62/C-04144 standard. After penetration tests, the grease is placed in a rolling apparatus, and the test is continued at 60℃ at 165 rpm for 4 h. Then a second penetration test is undertaken. Mechanical stability is determined from the difference in penetration values before and after the rolling process. The viscosity curves of the tested greases are obtained using an Anton Paar Physica MCR 102 rotational rheometer equipped with an air diffusion bearing connected to a pneumatic supply: an oil-free Jun-Air compressor and an air drying block. Rheoplus software controls the rheometer and analyze the measurement data. The measurements are taken in a cone-plate configuration (25 mm, 2°) with a constant measurement gap of 106 μm, within a shear rate range of 0.01–300 s^{-1} (600 measurement points) at 20℃ and 40℃ in three measurement series. A temperature of 20°C corresponds to laboratory conditions and allows for the comparison of the properties of different lubricant compositions and the comparison of the obtained results with other literature studies. The temperature of 40°C was chosen as representative of the conditions prevailing in the friction pair during tribological tests in a four-ball system. Therefore, adopting 40°C as the rheological measurement temperature allows for the assessment of the lubricant properties within a range corresponding to the actual heating during system operation. Before each measurement, the system temperature is stabilized for 5 min. Viscosity curves serve to assess the rheological properties, used to determine the yield stress (Casson model).

2.5. Tribological tests

A T-02 four-ball tester with the ability to measure the temperature of the friction node serves to determine the tribological properties of the tested lubricant compositions. The test elements are balls with a diameter of 12.7 mm, made of ŁH 15 bearing steel, with a surface roughness of Ra = 0.32 μm, and a hardness of 60–65 HRC. Anti-seizure parameters are determined using the following parameters: weld load (WL), scuffing load (SL), the limiting load of seizure (LLS), and the limiting pressure of seizure (LPS). The weld load (WL) is measured in accordance with the PN-76/C-04147 standard. This test involves running a set of four balls for 10 s in the presence of lubricant under increasingly higher loads until the balls welded. Lubrication properties under conditions of continuously increasing load are measured according to a methodology developed at the Łukasiewicz Research Network - Institute for Sustainable Technology. The test is conducted with a load linearly increasing from 0 to 7200 N over 18 s, at a spindle speed of 500 rpm and a load ramp rate of 409 N/s. When the friction torque suddenly increases, the node load level is referred to as the scuffing load (SL). Measurements continue until the limiting friction torque of 10 Nm or the maximum device load of 7200 N is reached. This point is referred to as the limiting load of seizure (LLS). The arithmetic mean of at least three measurements is used as the final result. The limiting pressure of seizure (LPS), a measure of the anti-seizure properties of greases under scuffing conditions, is calculated based on the LLS value, the wear scar diameter (d), and a factor taking into account the distribution of forces in the friction node (0.52), according to Eq. (1).

$$LPS = 0.52 \bullet \frac{LLS}{d^2} \quad (1)$$

The anti-seizure properties of the tested greases are determined by establishing the limiting load of wear (LLW). For this purpose, tests are conducted in accordance with the WTWT-94/MPS-025 guidelines at a constant load of 392.4 N, a ball speed of 500 rpm/min, and a test duration of 3600 s. The LLW parameter is a measure of the grease's resistance to wear and is calculated based on a coefficient that takes into account the force distribution in the friction node (0.52), the load value, and the diameter of the wear scars (d), according to Eq. (2).

$$LLW = 0.52 \bullet \frac{392.4}{d^2} \quad (2)$$

A Keyence 3D microscope serves to image the resulting scars and determine the surface roughness parameters of the scars on the test balls. Surface roughness is determined on the basis of the parameters S_a, S_z, S_p, S_v, and S_{sk}. The arithmetic mean surface height S_a is a parameter defining the average absolute value of the height of surface points relative to a reference plane. The maximum surface height S_z is the height difference between the highest (S_p) and lowest (S_v) points on an analyzed surface. The skewness parameter S_{sk} shows the asymmetry of height distribution on a trace surface. A positive value of the S_{sk} parameter indicates that a studied surface is dominated by peaks. A negative value indicates that a studied surface is dominated by valleys.

3. Results and discussion

3.1. The characteristics of carbon materials

The carbon materials were compared in terms of their structure using Raman spectroscopy, the presence of surface functional groups using FTIR spectroscopy, and the specific surface area based onN_2 adsorption/desorption isotherms. Additionally, the resulting biochar is analyzed for moisture and ash content using the gravimetric method by heating the sample at 105°C and 815°C, respectively, as well as for its chemical composition (EDS).

The BW biochar is characterized by a moisture content of 2.815 ± 0.050 % and an ash content of 10.940 ± 0.020 $\%_{dm}$. Our ash content results correlate quite well with the EDS results. This analysis reveals the presence of various elements on the BW biochar surface, primarily carbon and oxygen (totaling 85 %). The ash components are primarily mineral elements such as silicon, calcium, magnesium, potassium, phosphorus, and sodium. The sum of these elements from the EDS analysis of biochar (excluding carbon, oxygen, and nitrogen) is over 8 %. The remaining content may consist of both carbon residues (e.g., when the material may contain more stable forms of carbon-graphite-like structures) and oxygen (originating from metal oxides present in the ash, e.g., SiO_2, CaO, or from residual functional groups). Similar ash content values in biochar samples produced by the pyrolysis of wheat straw at 500°C were also obtained by other authors: 12.5–13.5 % (Zhang et al., 2022), 11 % (Ghorbani et al., 2022), 12.7 % (Kloss et al., 2012).

The structure of the carbon materials is analyzed using Raman spectrometry. The spectra are shown in Fig. 1.

Two peaks can be observed in the recorded spectrum for the graphite sample: a G band (first-order) and a 2D band (second-order). In the case of biochar, two peaks originating from the D and G bands are observed. The G band (1586 cm^{-1}) is associated with the in-plane $E_{2\,g}$ mode of single-crystalline graphitic carbon atoms in the honeycomb lattice. The D band (1358 cm^{-1}) reveals the presence of defects in the graphite lattice with $A_{1\,g}$ symmetry. The presence of the 2D band (2692 cm^{-1}) results from the double resonance activation mechanism of the D peak. The absence of the D band and the presence of the 2D band in the graphite spectrum indicate that it is a purely crystalline, defect-free graphite (Beyssac and Lazzeri, 2012; Reich and Thomsen, 2004). Information about in-plane defects and the disordered structure of biochar can be inferred from the I_D/I_G ratio. The calculated ratio of the D and G peak intensity heights for the BW sample is 0.0684 ± 0.0070. This is a very low value, indicating a highly ordered structure. Such low I_D/I_G ratio values have been observed in available literature data regarding Raman analyses of graphite samples. Vidoeski et al. obtained an I_D/I_G

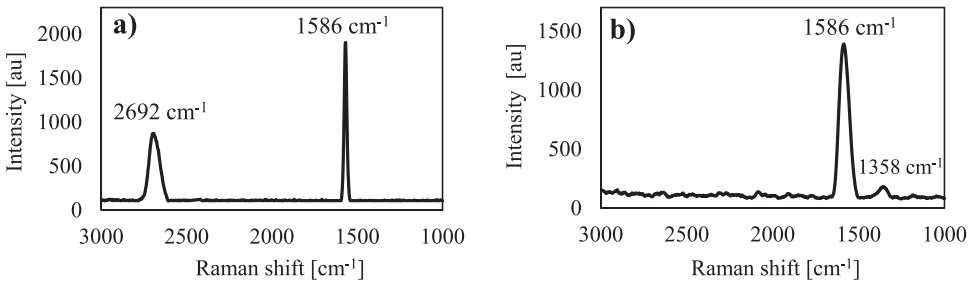

Fig. 1. Comparison of Raman spectra for carbon materials: graphite (a) and biochar (b).

ratio of 0.06 for highly ordered pyrolytic graphite (HOPG), which is a pure and ordered form of synthetic graphite (Vidoeski et al., 2016). Similar I_D/I_G values were also obtained by other authors studying natural graphite powder: 0.04 (Kim et al., 2013), 0.05 (Ostyn et al., 2021), 0.13 (Gu et al., 2013). Comparing our values for samples BW and G and the available literature data for graphite, it can be concluded that the biomass and pyrolysis process were selected correctly, as they generated a material with a graphite-like structure.

Fourier transform infrared (FTIR) spectroscopy analysis serves to identify surface functional groups. The FTIR spectra of graphite and biochar obtained from straw, following pyrolysis in a nitrogen atmosphere at 500°C, are shown in Fig. 2.

The FTIR spectroscopic spectrum of the analyzed commercial graphite shows a band at 1991 cm^{-1}, which can be attributed to the stretching vibrations of C═O (carbonyl) bonds (Kozdrach and Radulski, 2025b; Ţucureanu et al., 2016). In turn, the band observed at 2102 cm^{-1} may correspond to the presence of alkyne groups (–C≡C) Nandiyanto et al., (2019)). In the FTIR spectrum for the BW sample, some characteristic bands can be observed, reflecting the presence of functional groups remaining after a partial degradation of the main lignocellulosic components, such as cellulose, hemicellulose, and lignin. A very weak but clearly defined narrow peak can be seen at a wavelength of approximately 3635 cm^{-1}. This is attributed to the stretching of O–H groups, which may originate from water physically adsorbed on the biochar surface. Although this signal is not typical for temperatures of 500°C, its presence may indicate moisture accumulated after pyrolysis, especially if the sample is exposed to humid air (Nazari et al., 2019). The presence of this band is also confirmed by gravimetric analyses, which indicated the presence of moisture at a level of approximately 3 %.

In the broader range of 3000–3600 cm^{-1}, an extended, broad band is observed, with a maximum at approximately 3300 cm^{-1}. This band is typical of O–H bond stretching, occurring in alcohols, phenols, and polysaccharide residues. The fact that this band is still present in biochar suggests that some hydroxyl groups survived the pyrolysis process or were transformed into more stable structures that still retain the ability to form hydrogen bonds (Behazin et al., 2015; Miller et al., 1998). Around 3050 cm^{-1} occurs a very weak signal, which can be attributed to C–H bond stretching in aromatic structures (Lawrinenko and Laird, 2015). Although there is no distinct peak at 2920 cm^{-1}, a slight deflection of the baseline is visible, which may indicate the presence of methyl and methylene groups – aliphatic fragments typical of cellulose and hemicelluloses. Their distinct weakening is typical of thermal decomposition of these compounds during pyrolysis (Behazin et al., 2015; Molenda et al., 2025b). The strongest signal in the mid-frequency region is located at 1586 cm^{-1} and corresponds to the stretching vibrations of C═C bonds in aromatic structures, which indicates the presence of lignin or its aromatization products (Özsin et al., 2019). A band resulting from an asymmetric stretching of carboxylate groups COO^- may also be present in the same range, especially when a symmetric band is also visible. In the spectrum of BW biochar, such a signal indeed appears – a distinct peak is observed at 1412 cm^{-1}, which is attributed to the symmetric stretching of the COO^- group. The presence of these groups is particularly interesting because at 500°C, some of the carboxyl groups (–COOH) are decomposed by decarboxylation. However, some of them can survive in a more stable form as carboxylate anions. Their source is most likely uronic acids – such as glucuronic or galacturonic acid – naturally present in hemicelluloses. Though partially decomposed during pyrolysis, their fragments may remain bound to the biochar surface in the form of COO^- (Vaghela et al., 2023). At a wavelength of 1379 cm^{-1}, a much weaker peak appears, which can be associated with the bending of C–H groups in the methyl organic residues. It may originate from undegraded cellulose, hemicelluloses, or methyl fragments of lignin. However, the low intensity of this band suggests that most aliphatic compounds were decomposed during the pyrolysis process (Nazari et al., 2019; Vaghela et al., 2023). There is no distinct peak in the 1158 cm^{-1} range, but a noticeable bend in the curve suggests the presence of a signal from C–O–C ether bridge vibrations, likely originating from cellulose and/or lignin residues. Right next to it, at 1095 cm^{-1}, there is a strong band that may represent both C–O bond stretching vibrations and overlapping C–O–C signals. Both the bands indicate that some ether bonds remained intact or were transformed into more stable forms present in the biochar structure (Behazin et al., 2015; Miller et al., 1998). In the lower range of the spectrum, below 900 cm^{-1}, characteristic peaks at 873, 810, 753, and 695 cm^{-1} stand out. These correspond to some out-of-plane vibrations of C–H bonds in aromatic rings, typical of condensed carbon structures formed as a result of lignin aromatization. The presence of these bands strongly confirms structural transformations occurring during pyrolysis, indicating the transformation of some organic compounds into more ordered aromatic systems, which impart hydrophobic properties to biochar and increase

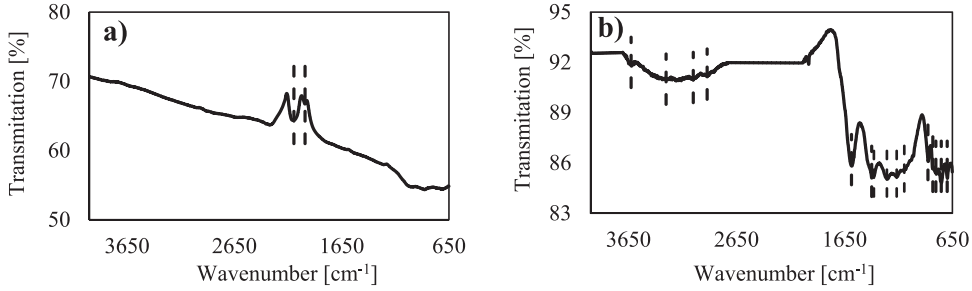

Fig. 2. Comparison of FTIR spectra for samples G (a) and BW (b).

its chemical stability Behazin et al., 2015; Vaghela et al., 2023).

The G and BW carbon materials are also analyzed when it comes to their specific surface area. The N_2 adsorption and desorption isotherms are shown in Fig. 3.

The isotherm obtained for the graphite sample, according to the IUPAC classification, is a type III isotherm. There is no clearly defined B inflection point, therefore, there is no identifiable monolayer formation. Adsorbent-adsorbate interactions are relatively weak, and adsorbed molecules cluster around the most favorable sites on the surface of a nonporous or macroporous solid (Thommes et al., 2015). However, the isotherm for the BW sample, according to the IUPAC classification, is a type II isotherm. These isotherms are characteristic of nonporous, macroporous, or low-surface-area materials. Their shape results from unconfined mono- and multilayer adsorption up to a high p/p_0. A sharp inflection of the isotherm plot is also be observed, which corresponds to the completion of monolayer coverage. Based on these obtained isotherms and using multipoint BET theory, the specific surface areas of 10.1 m^2/g for G and 177.4 m^2/g for BW are determined. These specific surface area values for graphite are close to those obtained by other authors: 7.7 m^2/g (Fouda et al., 2021), 8.2 m^2/g (Naboka et al., 2021), 4.2 m^2/g and 15.2 m^2/g (Blyth et al., 2000), ~15 m^2/g (Mohan et al., 2020). Also, in the case of biochars, these values are close to the results for biochars obtained by the pyrolysis of various lignocellulosic biomasses. Liu et al. arrived at a specific surface area of 201.3 m^2/g and 212.6 m^2/g for biochars produced at 500°C from corn stalks and cobs, respectively (Liu et al., 2014). Similar values were shown by Wijitkosum and Jiwnok for biochar made of cassava stems – 200 m^2/g (Wijitkosum and Jiwnok, 2019). On the other hand, Srinivasan and Sarmah obtained green waste biochar with a specific surface area of 153 m^2/g (Srinivasan and Sarmah, 2015). Maple biochar studied by Choudchury and Lansing was characterized by a specific surface area of 161 m^2/g (Choudhury and Lansing, 2020). However, literature data on biochar from wheat straw show very diverse results – from several m^2/g to approximately 100 m^2/g (Ćwieląg-Piasecka et al., 2023; Sieradzka et al., 2022; Wang et al., 2022; Wystalska and Kwarciak-Kozłowska, 2021; Zhao et al., 2013).

In summary, the parameters we assumed for the wheat straw pyrolysis process were correct. The pyrolysis process yielded a biochar material characterized by an ordered structure while retaining oxygen-containing surface functional groups. The resulting material has a moisture content of approximately 3 %, an ash content of 11 %, and a specific surface area of 177.4 m^2/g. Based on the parameters of BW biochar, it can be concluded that it can potentially be used as a modifier for mineral oil-based lubricants. The increased specific surface area compared to graphite and the presence of oxygen groups may have a beneficial effect on lubricant properties.

3.2. Assessment of the dispersion homogeneity of carbon additives in the grease matrix

Mineral greases with BW biochar (1 %, 3 %, 5 %) and G graphite (1 %, 3 %, 5 %) additives are prepared according to the methodology given in 2.3. In order to assess the homogeneity of dispersion of carbon additives, the prepared grease compositions are spread as a thin layer on microscope slides and imaged using a Keyence 3D microscope. Illustrative images obtained at 500x magnification are shown in Fig. 4.

Based on the images of lubricant compositions, it can be concluded that the adopted methodology for preparing mineral greases with BW and G additives is appropriate. Based on the obtained images, it can be concluded that the BW and G additives are evenly distributed throughout the lubricant compositions. Additional sizing of the carbon particle size was performed at 1000x magnification and confirmed the absence of agglomeration in the grease structure. The correctness of the grease composition preparation procedure was also confirmed in our previous studies using computed tomography (Molenda et al., 2025a).

3.3. Rheological properties

To determine the consistency class of the greases, penetration measurements are performed on the tested lubricant compositions after 60 kneading cycles. Mechanical stability tests were also conducted to determine changes in the structure of the tested greases caused by shear forces. The results are presented in Fig. 5.

The consistency class of the greases is assessed based on the NLGI classification. The base grease, with a penetration value of 260.67 ± 0.58 mm/10, can be classified as Class 1/2. All the other greases, with both BW and G additives, have penetration values above 265 mm/10. These greases are classified as NLGI Class 2. They are characterized by moderate hardness, sufficiently compact to adhere to surfaces, yet soft enough to spread and flow well.

Mechanical stability studies have shown that the introduction of carbon additives to the structure of mineral greases increases their stability. An increase in penetration values after rolling was observed in all greases tested. Both carbon additives have a graphite or graphite-like structure, which can strengthen the lithium soap network by penetrating between its fibers, thereby minimizing friction between the fibers and preventing fiber breakage. This results in favorable changes to mechanical stability compared to the base grease. However, the operating mechanisms of the additives vary. In the case of the BW additive, as its concentration in the grease increases, the resulting lubricant composition becomes more mechanically stable. The opposite trend is observed for the addition of graphite; with growing graphite concentration, greater changes in the grease's consistency are observed after rolling. Biochar, a porous material containing polar oxygen groups, adsorbs base oil more strongly to its surface, making the grease structure more resistant to shear. However, comparing the BW and G additives, the most similar results are noted for the 3 % additive concentrations: 4.28 ± 0.36 % and 4.78 ± 0.54 %, respectively.

The next stage of the rheological tests is to determine the yield point at temperatures of 20°C and 40°C. This parameter is determined based on the flow curves of the tested greases using the Casson rheological model. The results are presented in Fig. 6.

The analysis of yield point values for the base grease (MG) and the grease modified with biochar (BW) and graphite (G) additives at 20°C and 40°C shows that the effect of carbon additives is not very variable, although some differences can be observed depending on the type of

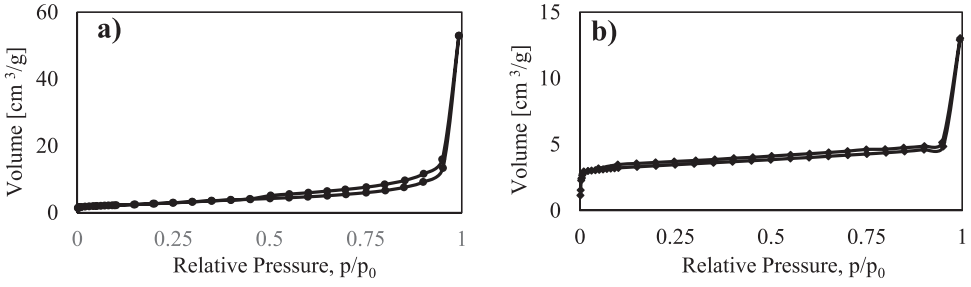

Fig. 3. Comparison of N_2 adsorption/desorption isotherms for G (a) and BW (b).

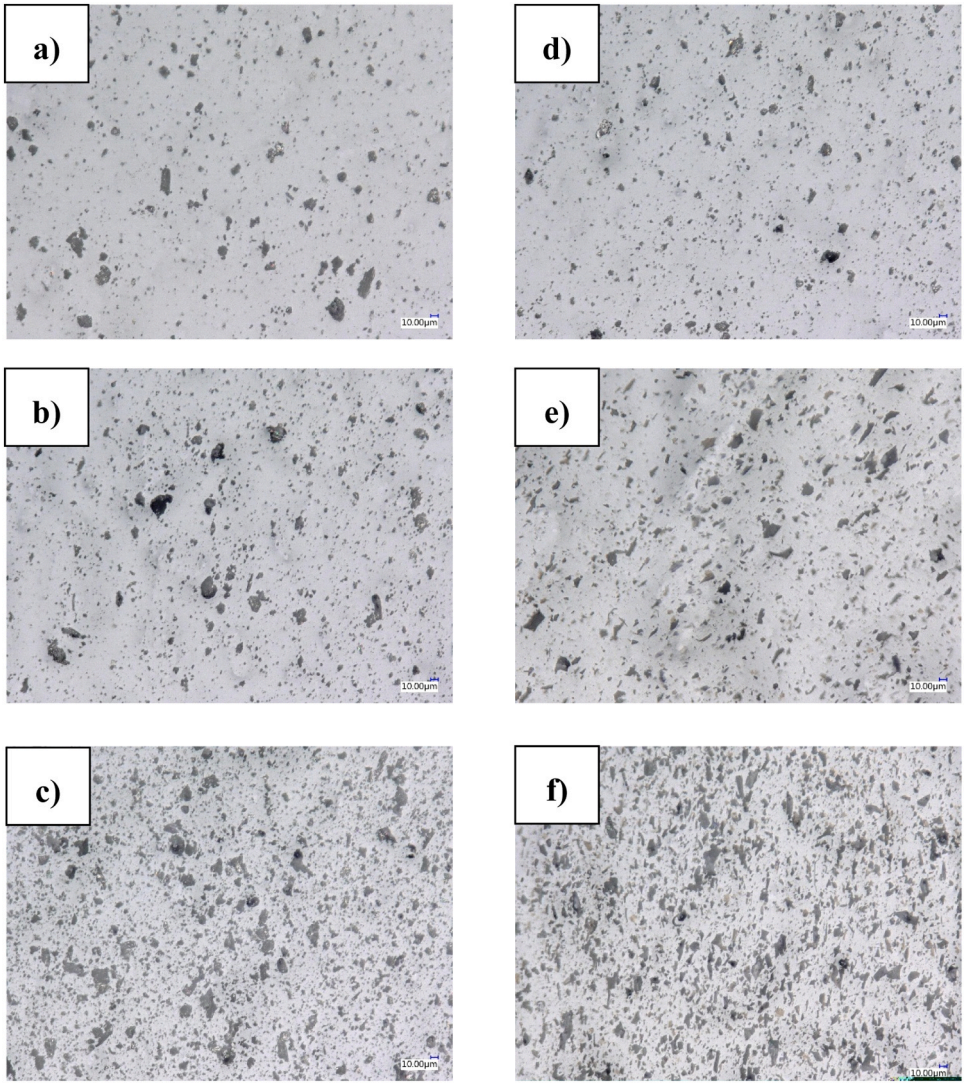

Fig. 4. The illustrative images of grease compositions with: a) 1 % BW, b) 3 % BW, c) 5 % BW, d) 1 % G, e) 3 % G, f) 5 % G.

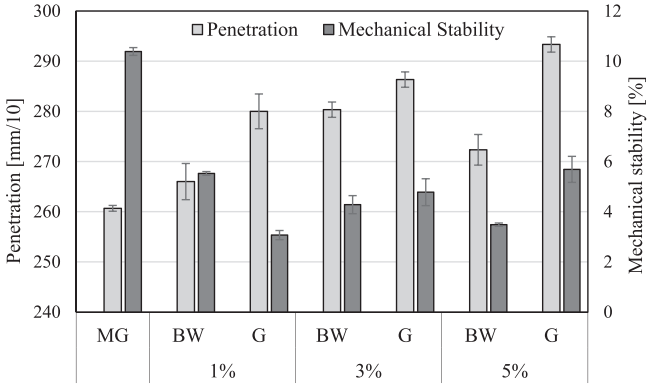

Fig. 5. The penetration and mechanical stability of the base grease and greases with BW and G additives.

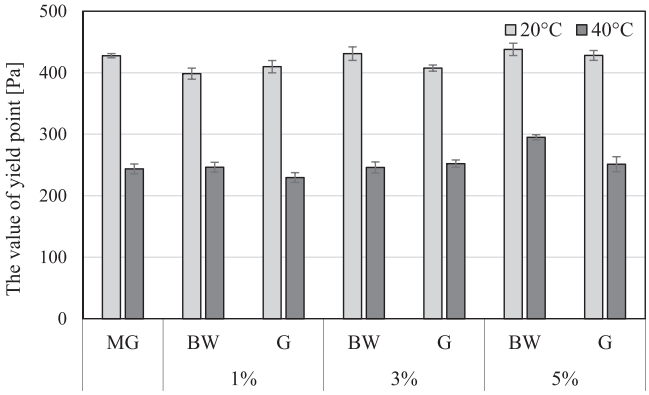

Fig. 6. Yield point values for mineral greases.

additive and its concentration. The MG grease has a yield point of 427.7 ± 3.4 Pa at 20°C and 244 ± 15 Pa at 40°C. Introducing a 1 % BW additive to the structure of the base mineral grease lowers the yield point to 398 ± 16 Pa (20°C) and 246 ± 25 Pa (40°C), indicating an initial fluidification of the lithium soap network due to oil adsorption on the porous biochar structure. 3 % BW increases this parameter to 431 ± 34 Pa (20°C) and it remains at 246 ± 25 Pa at 40°C, while at 5 % BW it reaches the highest values of 438 ± 21 Pa (20°C) and 295 ± 28 Pa (40°C). In the case of graphite, a reduction in the yield point is observed for 1 % G (409.8 ± 5.0 Pa at 20°C and 230 ± 15 Pa at 40°C) and 3 % G (408 ± 23 Pa at 20°C) compared to the base grease. For 3 % and 5 % G, an increase in the yield point at 40°C is observed – 252.1 ± 4.2 Pa and

251 ± 12 Pa, respectively. However, in the case of 5 % G at 20°C, the yield point (428 ± 19 Pa) returns to the value achieved for the base grease.

A linear relationship between the additive concentration and the yield point can only be observed in studies conducted at 20°C with the addition of biochar (R^2=0.87). In the remaining cases, no such relationship exists. Our previous studies indicate that the effect of biochar additives on the yield point can be nonlinear and concentration-dependent [15]. Kozdrach and Radulski observed that a small addition of biochar (1 %) significantly lowers the yield point. When the concentration rises to 3 %, the yield point may increase, then, when the additive concentration increases to 5 %, the yield point is significantly reduced (Kozdrach and Radulski, 2025a). Graphite, on the other hand, typically lowers the yield point compared to the base grease. Czarny and Paszkowski, studying lithium greases, demonstrated that the addition of graphite particles reduces the shear stresses (including the yield point) of the system (Czarny and Paszkowski, 2007). This is also confirmed by our results: 1–3 % G results in a slightly lower yield point than the base grease (e.g., from 427 Pa to ~408–410 Pa), while 5 % G results in a value close to the base value. Furthermore, research into nanomaterials in lithium greases (e.g., graphene addition) indicates that very small, well-dispersed carbon particles can compress the thickener structure and enhance its viscoelastic properties. However, our studies suggest that graphite of a size of several tens of microns does not achieve such densification, but rather induces network relaxation.

Comparing carbon additives of the same concentration, it can be observed that there are no significant differences in the results obtained for 1 % (398.5 ± 9.0 Pa for BW and 409.8 ± 5.0 Pa for G) and 5 % (438 ± 11 Pa for BW and 428.1 ± 8.0 Pa for G) at 20°C and for 3 % (246.0 ± 8.0 Pa for BW and 252.1 ± 4.2 Pa for G) at 40°C. The largest differences are observed for additives of 5 % concentration at 40°C - 295.0 ± 9.0 Pa for BW and 251 ± 12 Pa for G. The mechanisms of interaction of carbon additives with the lithium soap network are different due to the particle structure. Amorphous biochar containing oxygenated groups can penetrate between lithium soap fibers or bind oil molecules, partially replacing the binder role and attaching an additional molecular network to the base oil chain (Kozdrach and Radulski, 2025b). This strengthens the grease structure, which can be observed as an improved resistance to deformation at 3–5 % BW. Graphite, on the other hand, as a chemically inert layered material, acts primarily mechanically. Its particles do not chemically interact with the lithium soap network but disperse, facilitating the separation of the lithium and oil networks. As a result, the addition of graphite weakens the cohesion of the lithium grease fibers and causes a reduction of the yield point (at low concentrations) or no significant change (at higher concentrations), without any major jumps in values. Unlike amorphous carbon, graphite forms layered films on surfaces rather than solid structures within the grease (Czarny and Paszkowski, 2007).

3.4. Tribological properties and wear scar characteristics

The anti-scuffing properties of the tested greases are assessed by analyzing the following parameters: weld load (WL), scuffing load (SL), limiting load of seizure (LLS), and limiting pressure of seizure (LPS). For the WL and LLS, no differences were observed between the values achieved for the base grease and the greases with carbon additives. For all the tested greases, the weld load value is 4905 N, and the limiting load of seizure is 7200 N. The values of SL and LPS are presented in Fig. 7.

For all the tested greases with carbon additives, the scuffing load (SL) declines compared to the base grease. This may be due to the hardness of the carbon particles and their irregular shape. The initial stage of their polishing due to friction may negatively impact the time until the first signs of scuffing compared to the base grease (Kumar et al., 2020b). However, considering the values of LPS (Fig. 7), the carbon additives used have a very beneficial effect on anti-scuffing properties. This effect varies and depends on the type of additive and its concentration. When

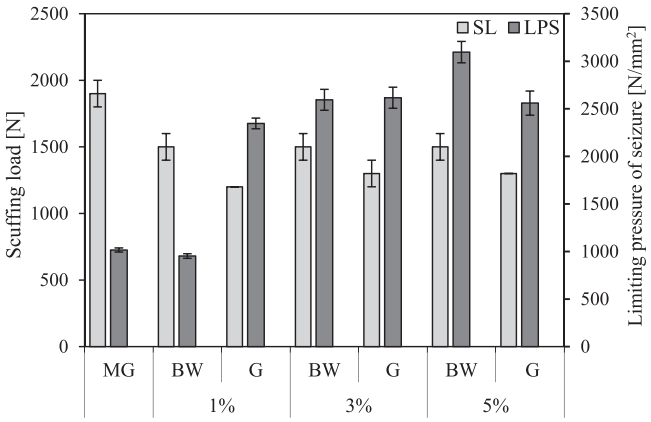

Fig. 7. The scuffing load and limiting pressure of seizure obtained for the tested greases.

biochar is used as an additive in mineral grease, LPS value rises while its concentration grows. For 1 % BW, the LPS value is lower than the base value for MG. It can be concluded that this concentration of BW is insufficient to improve anti-scuffing properties. Increasing the BW concentration to 3 % raises the LPS value to 2595 ± 220 N/mm² (a 155 % increase compared to MG). Further increasing the BW concentration brings the LPS even higher – 3096 ± 113 N/mm² (a 205 % increase compared to MG). In the case of graphite, such a relationship is not observed. The LPS value for 1 % G is 2347 ± 56 N/mm². However, for 3 % and 5 % graphite, similar values are generated– 2617 ± 111 N/mm² and 2560 ± 127 N/mm², respectively. For all the graphite concentrations tested, the LPS value rises considerably compared to the base grease, by 131 %, 158 %, and 152 % for 1 %, 3 %, and 5 % G, respectively.

Comparing the results for various carbon additives at the same concentrations, with a 1 % addition, more favorable values are obtained for the graphite additive, an increase in LPS values by 146 % compared to 1 % BW. For the 3 % concentration, the LPS values are similar – 2595 ± 100 N/mm² for BW and 2617 ± 111 N/mm² for G. However, at a 5 % concentration, higher values were observed for the biochar additive –LPS values are 21 % greater than for the graphite additive.

Based on these results, it can be concluded that, in terms of the limiting pressure of seizure, the optimal graphite concentration is 3 %. There are numerous scientific studies confirming the effectiveness of graphite as an additive that improves anti-scuffing properties (e.g. Azman et al., 2024; Kamis et al., 2024; Kumar et al., 2020a; Kumar et al., 2021; Tan et al., 2022). Comparing our results for BW and G, it can be concluded that, in terms of anti-scuffing properties, biochar, an ecological material, can be successfully used as a replacement for graphite additives in mineral greases thickened with lithium stearate. A complete replacement of graphite with biochar while maintaining anti-scuffing properties is possible for a 3 % additive concentration (3 % G - 2617 ± 111 N/mm², 3 % BW - 2595 ± 220 N/mm²). However, increasing the BW additive concentration to 5 % can further significantly raise LPS values (by 18 % compared to 3 % G).

In order to assess anti-wear properties, tribological tests of the tested greases are carried out at a constant friction node load of 392.4 N. Based on the diameters of the scar wear, the limiting load of wear (LLW) values are determined, shown in Fig. 8.

Based on the obtained data, it can be observed that the LLW depends on the type of carbon additive used and its concentration. The LLW values for greases with BW additive, its values are 1277 ± 64 N/mm², 1493 ± 81 N/mm², and 1584 ± 176 N/mm² for 1, 3, and 5 % G, respectively. For the graphite additive, they are 757 ± 58 N/mm², 550 ± 36 N/mm², and 455 ± 27 N/mm² for 1, 3, and 5 % G, respectively. In both cases, very strong linear correlations are observed at the assumed significance level of 0.05. r coefficients for the dependence of the LLW

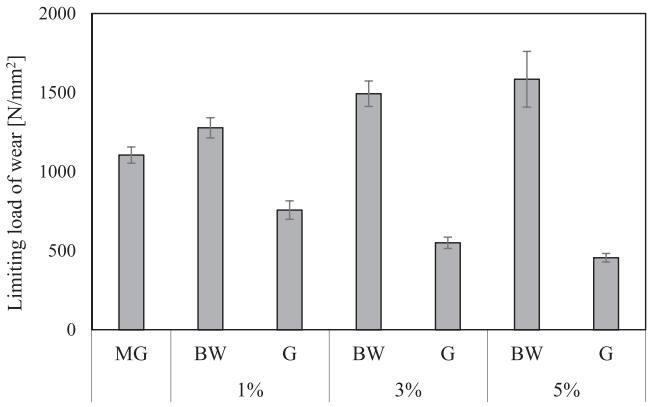

Fig. 8. The limiting load of wear of a tribological system lubricated with the tested greases.

value on the concentration of BW and G additives are 0.989 and −0.966, respectively. For greases with BW additive, the LLW value increases with growing BW concentration. The use of biochar raises the limiting load of wear by 15 %, 35 %, and 43 % for 1 %, 3 %, and 5 % BW, respectively, compared to the base grease, for which the LLW is 1105 ± 51 N/mm^2. However, for the G additive, a negative r coefficient was obtained, indicating that the LLW diminishes with increasing additive concentration. The LLW falls by 31 %, 50 %, and 59 % for 1 %, 3 %, and 5 % G, respectively, compared to the base grease. Comparing the LLW values obtained for the same concentrations of carbon additives, it was observed that in each case the results obtained with the biochar additive are more favorable than for the graphite additive – an increase of 69 % for 1 %, 171 % for 3 %, and 248 % for 5 %. The graphite used in the research is used in commercial mineral greases designed especially for the automotive industry, including truck fifth wheels. Operating conditions for such grease include high surface pressures (the total weight of the trailer and the dynamic forces during starting, braking, and turning cause very high loads), low relative speed, and boundary lubrication (the oil film may be very thin or broken in places, especially under heavy loads) (Graco, 2025; Shell, 2025). Therefore, the additives used in such greases must primarily fulfill anti-seize functions. Graphite is a widely known and used EP (extreme-pressure) additive for greases (Morstein and Dienwebel, 2021). Excellent anti-seize properties characterize it. However, this effect depends on many factors, including their origin, purity, granulation, and shape (Harne et al., 2022; Tamashausky, 2002). Its main function is to protect metal surfaces from seizure under high pressures or boundary lubrication, i.e., in conditions where the oil film is broken. To provide anti-wear properties, graphite is often used in combination with molybdenum disulfide, which is also primarily an anti-seize additive, but also possesses anti-wear properties (EP/AW). The synergistic effect of these additives provides the grease with a broader range of anti-seize protection (from moderate to very high loads) across a wider operating temperature range and in various environmental conditions (Vazirisereshk, 2019). Our research has shown that biochar obtained from the pyrolysis of wheat straw can be used as a graphite additive replacement, as it has excellent anti-seize properties and significantly improves the anti-wear properties of mineral oil-based greases, eliminating the need to add molybdenum disulfide.

To characterize the tribological wear mechanism, the wear scar of steel balls is visualized after tribological tests conducted at a constant load of the friction node (Fig. 9), and their surface roughness is analyzed, including the determination of S_a, S_z, S_p, S_v, and S_{sk} (Table 1).

Based on the wear scar images, it can be concluded that the primary tribological wear mechanism in all cases is grooved wear. This typically results from the plastic deformation of a material under the influence of abrasive grains, used as carbon additives in the tested greases. Only some minor irregularities can be observed with BW as an additive. However, with graphite, the resulting V-shaped grooves are significantly deeper, and material deposition is observed at the outer edges of the trace. Furthermore, pitting is also noted for the highest graphite concentration.

Based on the roughness results, the roughness values do not differ with the biochar additive. For the BW additive, the S_a values are3.47 ± 0.60 μm, 2.43 ± 0.66 μm, and 4.61 ± 0.48 μm for 1 %, 3 %, and 5 % BW, respectively, and the S_z values are 13.3 ± 2.7 μm, 9.6 ± 3.0 μm, and 18.1 ± 2.5 μm, respectively. This trend in the result distribution is also maintained for the other analyzed parameters. This means a reduction in roughness by 70 %, 79 %, and 60 %, respectively, compared to the MG base grease. The roughness values obtained for the

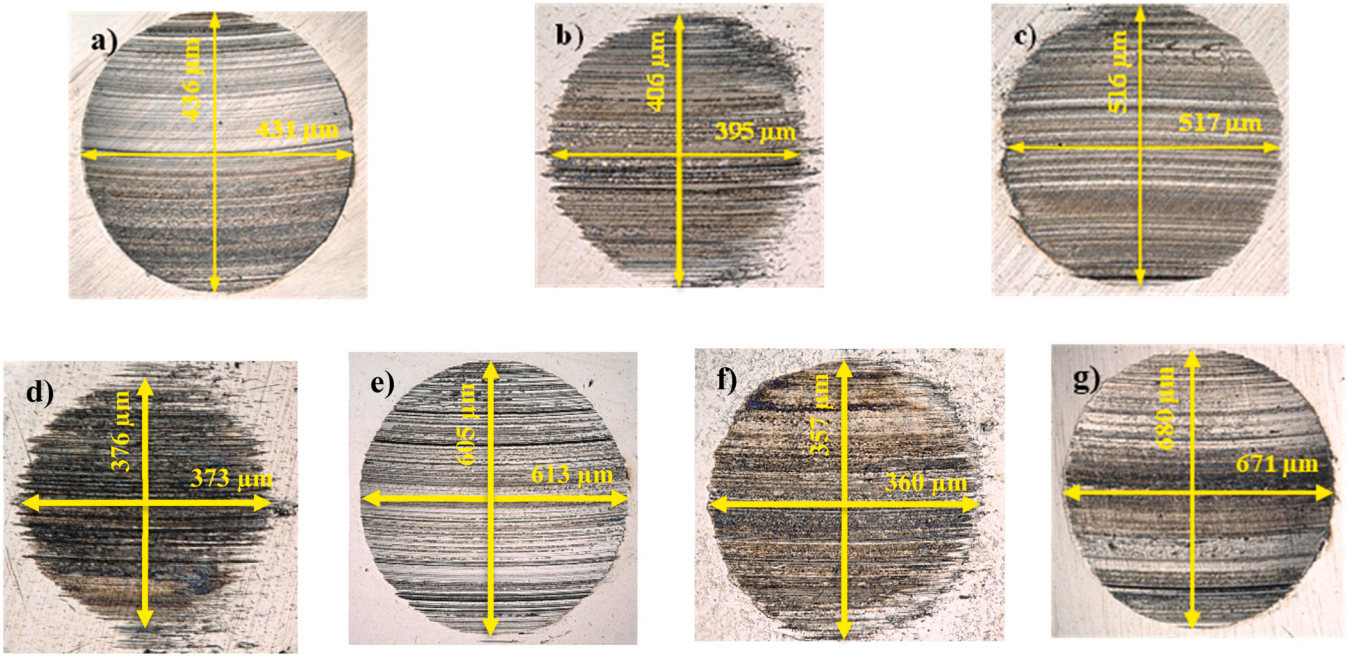

Fig. 9. The images of wear scar after the tribological testing of greases: a) MG, b) 1 % BW, c) 1 % G, d) 3 % BW, e) 3 % G, f) 5 % BW, g) 5 % G.

Table 1
Surface roughness parameters of wear scar after tribological tests.

Parameters	MG	1 % BW	1 % G	3 % BW	3 % G	5 % BW	5 % G
S_a [μm]	11.5 ± 1.6	3.47 ± 0.60	4.69 ± 0.52	2.43 ± 0.66	10.5 ± 1.0	4.61 ± 0.48	12.42 ± 0.79
S_z [μm]	48.8 ± 2.0	13.3 ± 2.7	18.2 ± 7.0	9.6 ± 3.0	36.9 ± 6.6	18.1 ± 2.5	41.1 ± 4.1
S_p [μm]	34.6 ± 3.7	9.3 ± 1.5	15.6 ± 6.8	6.1 ± 1.4	27.6 ± 4.9	13.6 ± 2.4	29.3 ± 3.1
S_v [μm]	14.2 ± 2.0	4.0 ± 1.3	2.59 ± 0.75	3.5 ± 1.5	9.2 ± 1.7	4.47 ± 0.32	11.9 ± 1.4
S_{sk}	0.53 ± 0.38	0.65 ± 0.14	1.98 ± 0.32	0.41 ± 0.19	0.83 ± 0.05	0.97 ± 0.18	0.54 ± 0.14

BW additive indicate that the tested scar surface can be classified as moderately rough. For the graphite additive, the roughness parameters S_a, S_z, S_p, and S_v increase with a growing graphite concentration. Comparing the roughness values obtained for the same concentrations of carbon additives, for each analyzed concentration, the scar wear surfaces after the tribological testing of greases with graphite additives exhibit a higher roughness compared to the scar wear surfaces after tests with greases including BW additives. The values obtained for 5 % G are similar to those obtained for the base grease. The positive surface skewness values obtained for all the tested wear scars indicate that peaks dominate the tested surfaces. These are the side effects of the groove formation process, where some of the removed material is deposited on groove edges. This is also confirmed by the results obtained for the S_p and S_v parameters. In all the traces, the S_p peak heights exceed the valley depths below the S_v surface core.

The biochar protective mechanism is likely the result of several overlapping processes, which ultimately lead to improved anti-wear and anti-scuffing properties in lithium stearate-thickened mineral greases. The irregular shape of biochar can produce a surface polishing effect, contributing to reduced wear scar roughness (Adeniyi et al., 2021), but also causes the formation of micro-cavities. These micro-cavities help retain oil in the shear zone, creating a thin protective layer that reduces local peak pressures and thus prevents micro-seizure (Kumar et al., 2020b). Ash contained in biochar can also settle in the depressions, reducing the depth of the valleys (a low Sv value), while simultaneously absorbing some of the load and thus providing additional surface protection against wear (Akhtar et al., 2016). Unlike graphite particles, BW biochar has polar oxygen groups that strongly adsorb oil and thickener molecules, forming a durable, thin protective film on metal contacts (Yu et al., 2023). Thanks to these mechanisms, mineral greases with biochar additives provide better anti-wear properties compared to graphite additives.

The proposed wear mechanism is also confirmed by our previous preliminary studies on the use of biochar as a lubricant additive (Molenda et al., 2025b). These studies demonstrated that adding biochar to mineral grease reduced friction, but XPS analysis revealed no significant differences in the spectral band positions recorded in the wear scar after tests with the base grease and the biochar grease. This indicates that no organic oxygen products form a boundary layer in the wear scar during friction under the test conditions. The decisive factor for the tribological properties is the presence of ordered graphite-like structures in the biochar, which facilitate lubricant interaction under friction conditions, rather than the formation of boundary layers (including lubricant components) that chemically bond with the tribosystem material.

4. Conclusion

The aim of the research presented in this article is to investigate the possibility of replacing graphite with biochar in mineral greases thickened with lithium stearate. This is an important issue because graphite is a critical raw material, meaning its availability and strategic importance are crucial to the economy. Graphite with a particle size below 35 μm, successfully used in commercially available mineral greases, is utilised for the study. Biochar is produced by the pyrolysis of wheat straw at 500°C. Both the carbon additives are compared in terms of their structure, the presence of functional groups, and specific surface area. The graphite used displays a low specific surface area and a lack of surface functional groups. The resulting biochar, on the other hand, has an ordered structure while retaining surface functional groups containing oxygen, a moisture content of approximately 3 %, an ash content of 11 %, and a specific surface area of 177.4 m^2/g. To evaluate the potential for replacing graphite with biochar and compare the effect of carbon additive concentration on the properties of mineral greases thickened with lithium stearate, lubricant compositions are prepared with varying concentrations of biochar and commercial graphite (1 %, 3 %, and 5 %).

The studies of the rheological and tribological properties of mineral greases thickened with lithium stearate demonstrate that biochar from wheat straw has significant potential as a graphite substitute. Among the parameters tested, the optimal concentration enabling a complete replacement of graphite with biochar is 3 %. Grease with 3 % BW added does not negatively influence rheological properties (3 % G: NLGI 2, mechanical stability – 4.78 ± 0.54 %, yield point at 20°C - 408 ± 10 Pa, yield point at 40°C – 252.1 ± 4.2 Pa; 3 % BW: NLGI 2, mechanical stability – 4.28 ± 0.36 %, yield point at 20°C - 431 ± 10 Pa, yield point at 40°C – 246.0 ± 8.0 Pa) and anti-scuffing properties (LPS values: 3 % G - 2617 ± 111 N/mm^2, 3 % BW - 2595 ± 220 N/mm^2) and significantly improves anti-wear properties (LLW values: 3 % G - 550 ± 36 N/mm^2, 3 % BW - 1493 ± 81 N/mm^2). On an industrial scale, to impart anti-wear properties, graphite requires the use of other additives, most commonly molybdenum disulfide. This compound occurs naturally in the environment as the mineral molybdenite, but the improper handling of MoS_2 causes soil and water contamination. Our results show that the BW additive has a positive effect on the anti-wear properties of mineral greases without requiring other additives.

The likely protective mechanism of biochar is a consequence of its specific properties, which impart beneficial properties to mineral greases. Irregular particle shapes and sharp edges can cause surface polishing on the one hand and the formation of micro-cavities on the other. The latter can serve a dual purpose: they can retain oil in the shear zone, leading to the formation of a protective layer, and they can serve as a deposition site for ash particles, which will absorb some of the load. The porosity of the biochar and the presence of polar oxygen groups on its surface also have a beneficial effect, strongly adsorbing oil and thickener molecules and creating a protective film on metal contacts.

The obtained research results also showed that replacing the graphite additive with eco-friendly biochar while maintaining the rheological and tribological properties of mineral lubricants eliminates the need for lengthy biochar grinding processes, which reduces the time and cost of pre-preparing biochar additives. The effect of biochar fraction size on the rheological and tribological properties of mineral lubricants thickened with lithium stearate will be the subject of our further, more detailed studies.

Data statement

Data sets are available at: https://doi.org/10.5281/zenodo.16925172

CRediT authorship contribution statement

Monika Łożyńska: Writing - review & editing, Writing - original draft, Visualization, Validation, Methodology, Investigation, Formal analysis, Data curation, Conceptualization. **Jarosław Molenda:** Writing - review & editing, Validation, Supervision, Project administration, Methodology, Funding acquisition, Conceptualization. **Rafał Kozdrach:** Writing - review & editing, Validation, Methodology, Investigation, Data curation. **Paweł Radulski:** Writing - review & editing, Writing - original draft, Validation, Investigation, Data curation. **Karolina Dziosa:** Methodology, Investigation, Data curation. **Monika Makowska:** Project administartion, Funding acquisition, Conceptualization.

Funding

This study was funded under a research project. The Use of carbonisate from waste lignocellulosic biomass as a substitute for non-renewable raw materials for the production of innovative biochar greases project is carried out within the Proof of Concept programme of the Foundation for Polish Science co-financed by the European Union under the European Funds for Smart Economy 2021–2027 (FENG).

Declaration of competing interest

The authors declare that they have no known competing financial interests or personal relationships that could have appeared to influence the work reported in this paper.

Declaration of Competing Interest

The authors declare the following financial interests/personal relationships which may be considered as potential competing interests: Jaroslaw Molenda reports financial support was provided by Foundation for Polish Science. If there are other authors, they declare that they have no known competing financial interests or personal relationships that could have appeared to influence the work reported in this paper.

Data availability

I have shared the link to my data at the Attach File step.

References

Adeniyi, A.G., Abdulkareem, S.A., Ighalo, J.O., Amosa, M.K., Popoola, A.O., Ogunniyi, S., Abdulkareem, M.T., 2021. Usage of biomass-based carbon materials as lubricant additive: effects on rheological and tribological properties. Lett. Appl. NanoBioSci. 10, 2861–2868. https://doi.org/10.33263/LIANBS104.28612868.

Akhtar, K., Khalid, H., Ul Haq, I., Malik, A., 2016. Improvement in tribological properties of lubricating grease with quartz-enriched rice husk ash. Tribol. Int. 93, 58–62. https://doi.org/10.1016/j.triboint.2015.09.015.

Azman, N.F., Samion, S., Paiman, Z., Hamid, M.K.A., 2024. Tribological performance and mechanism of graphite, hBN and MoS2 as nano-additives in palm kernel oil-based lubricants: a comparative study. J. Mol. Liq. 410, 125616. https://doi.org/10.1016/j.molliq.2024.125616.

Barszcz, W., Łożyńska, M., Molenda, J., 2024. Impact of pyrolysis process conditions on the structure of biochar obtained from apple waste. Sci. Rep. 14, 10501. https://doi.org/10.1038/s41598-024-61394-8.

Behazin, E., Ogunsona, E., Rodriguez-Uribe, A., Mohanty, A.K., Misra, M., Anyia, A.O., 2015. Mechanical, chemical, and physical properties of wood and perennial grass biochars for possible composite application. BioResources 11, 1334–1348. https://doi.org/10.15376/biores.11.1.1334-1348.

Beyssac, O., Lazzeri, M., 2012. Application of Raman spectroscopy to the study of graphitic carbons in the Earth Sciences. In: Dubessy, J., Caumon, M.-C., Rull, F. (Eds.), Applications of Raman spectroscopy to earth sciences and cultural heritage. European Mineralogical Union and the Mineralogical Society of Great Britain & Ireland, London, pp. 415–454.

Blyth, R.I.R., Buqa, H., Netzer, F.P., Ramsey, M.G., Besenhard, J.O., Golob, P., Winter, M., 2000. XPS studies of graphite electrode materials for lithium ion batteries. Appl. Surf. Sci. 167, 99–106. https://doi.org/10.1016/S0169-4332(00)00525-0.

Choudhury, A., Lansing, S., 2020. Biochar addition with Fe impregnation to reduce H2S production from anaerobic digestion. Bioresour. Technol. 306, 123121. https://doi.org/10.1016/j.biortech.2020.123121.

Ćwieląg-Piasecka, I., Jamroz, E., Medyńska-Juraszek, A., Bednik, M., Kosyk, B., Pollákova, N., 2023. Deashed Wheat-Straw Biochar as a Potential Superabsorbent for Pesticides. Materials 16, 2185. https://doi.org/10.3390/ma16062185.

Czarny, R., Paszkowski, M., 2007. The influence of graphite solid additives, MoS2 and PTFE on changes in shear stress values in lubricating greases. J. Synth. Lubr. 24, 19–29. https://doi.org/10.1002/jsl.26.

ECGA, 2022. Graphite - A strategic raw material, indispensable to implementing the EU, regional and national policies, achieving the climate targets and overcoming the current energy-related crisis. European Advanced Carbonand Graphite Association.

Fouda, A.N., Duraia, E.S.M., Almaqwashi, A.A., 2021. Facile and scalable green synthesis of N-doped graphene/CNTs nanocomposites via ball milling. Ain Shams Eng. J. 12, 1017–1024. https://doi.org/10.1016/j.asej.2020.04.011.

Ghorbani, M., Li, Q., Kianmehr, M.H., Arabhosseini, A., Sarlaki, E., Vakilian, K.A., Varjani, S., Wang, Y., Wei, D., Pan, J., Aghbashlo, M., Tabatabaei, M., 2022. Highly digestible nitrogen-enriched straw upgraded by ozone-urea pretreatment: digestibility metrics and energy-economic analysis. Bioresour. Technol. 360, 127576. https://doi.org/10.1016/j.biortech.2022.127576.

Gotore, O., Masere, T.P., Muronda, M.T., 2024. The immobilization and adsorption mechanisms of agro-waste based biochar: a review on the effectiveness of pyrolytic temperatures on heavy metal removal. Environ. Chem. Ecotoxicol. 6, 92–103. https://doi.org/10.1016/j.enceco.2024.04.002.

Graco, 2025. The Importance of a Properly Lubricated Fifth Wheel Top Plate. Technical Report, last access 17.11.2025. Avalaible on: ⟨https://www.graco.com/us/en/vehicle-service/solutions/articles/the-importance-of-a-properly-lubricated-fifth-wheel-top-plate.html⟩.

Gradziuk, P., Gradziuk, B., Trocewicz, A., Jendrzejewski, B., 2020. Potential of straw for energy purposes in poland—forecasts based on trend and causal models. Energies 13, 5054. https://doi.org/10.3390/en13195054.

Gu, C., Zhang, H., Wang, X., Tu, J., 2013. Synthesis of reduced graphene oxide by an ionothermal method and electrochemical performance. RSC Adv. 3, 11807. https://doi.org/10.1039/C3RA41485J.

Guan, W., Hou, X., Wang, Y., Chu, C., Ali, M.K.A., 2025. Interaction lubrication mechanism between nano-biochar and traditional oil additives under various sliding conditions. Lubricants 13, 102. https://doi.org/10.3390/lubricants13030102.

Harne, M.S., Nagare, P.N., Ghalme, S.G., Pawar, A.M., Patil, S.S., Kadam, J.J., Bamane, K.D., Londhe, P.V., 2022. Improvement of lithium grease tribological performance with graphite as an additive. Ciência Eng. Sci. Eng. J. 10, 36–47. https://doi.org/10.52783/cienceng.v10i1.17.

Holmberg, K., A. Erdemir, A., 2017. Influence of tribology on global energy consumption, costs and emissions. Friction 5, 263–284. https://doi.org/10.1007/s40544-017-0183-5.

Kamis, S.L., Yusoff, B.I., Fukuda, K., Tahir, N.A.M., Sukri, I.A.A., Ahmad, M.A., 2024. Tribological properties of graphite particles as an anti-friction and anti-wear additive in lithium soap grease. J. Tribol. 40, 179–198.

Kaźmierczak, B., Molenda, J., Swat, M., 2021. The adsorption of chromium (III) ions from water solutions on biocarbons obtained from plant waste. Environ. Technol. Innov. 23, 101737. https://doi.org/10.1016/j.eti.2021.101737.

Kim, S.G., Park, O.K., Lee, J.H., Ku, B.C., 2013. Layer-by-layer assembled graphene oxide films and barrier properties of thermally reduced graphene oxide membranes. Carbon Lett. 14, 247–250. https://doi.org/10.5714/CL.2013.14.4.247.

Kloss, S., Zehetner, F., Dellantonio, A., Hamid, R., Ottner, F., Liedtke, V., Schwanninger, M., Gerzabek, M.H., Soja, G., 2012. Characterization of slow pyrolysis biochars: effects of feedstocks and pyrolysis temperature on biochar properties. J. Environ. Qual. 41, 990–1000. https://doi.org/10.2134/jeq2011.0070.

Kozdrach, R., Radulski, P., 2025b. Influence of a walnut shell biochar additive on the tribological and rheological properties of vegetable lubricating grease. Lubricants 13, 213. https://doi.org/10.3390/lubricants13050213.

Kozdrach, R., Radulski, P., 2025a. Application of chokeberry biochar as a modified additive to the vegetable lubricants: the tribological and rheological properties. Sci. Rep. 15 (1), 3964. https://doi.org/10.1038/s41598-025-87374-0.

Kumar, N., Saini, V., Bijwe, J., 2020a. Performance properties of lithium greases with PTFE particles as additive: controlling parameter- size or shape? Tribol. Int. 148, 106302. https://doi.org/10.1016/j.triboint.2020.106302.

Kumar, N., Saini, V., Bijwe, J., 2020b. Tribological investigations of nano and micro-sized graphite particles as an additive in lithium-based grease. Tribol. Lett. 68, 124. https://doi.org/10.1007/s11249-020-01362-1.

Kumar, N., Saini, V., Bijwe, J., 2021. Synergism or antagonism in tribo-performance of nano-greases using combinations of nanoparticles of graphite and PTFE. Appl. Nanosci. 11, 2525–2536. https://doi.org/10.1007/s13204-021-02099-6.

Larsson, E., Westbroek, R., Leckner, J., Jacobson, S., Rudolphi, Å.K., 2021. Grease-lubricated tribological contacts – Influence of graphite, graphene oxide and reduced graphene oxide as lubricating additives in lithium complex (LiX)- and polypropylene (PP)-thickened greases. Wear 486–487, 204107. https://doi.org/10.1016/j.wear.2021.204107.

Lawrinenko, M., Laird, D.A., 2015. Anion exchange capacity of biochar. Green. Chem. 17, 4628–4636. https://doi.org/10.1039/C6GC00828J.

Li, Z., He, Q., Du, S., Zhang, Y., 2020. Effect of few layer graphene additive on the tribological properties of lithium grease. Lubr. Sci. 32, 333–343. https://doi.org/10.1002/ls.1506.

Liu, Y., Yu, S., Shi, Q., Ge, X., Wanga, W., 2022. Graphene-family lubricant additives: recent developments and future perspectives. Lubricants 10 (9), 215. https://doi.org/10.3390/lubricants10090215.

Liu, X., Zhang, Y., Li, Z., Feng, R., Zhang, Y., 2014. Characterization of corncob-derived biochar and pyrolysis kinetics in comparison with corn stalk and sawdust. Bioresour. Technol. 170, 76–82. https://doi.org/10.1016/j.biortech.2014.07.077.

Makowska, M., Dziosa, K., 2024. Influence of different pyrolysis temperatures on chemical composition and graphite-like structure of biochar produced from biomass of green microalgae *Chlorella sp.* Environ. Technol. Innov. 35, 103667. https://doi.org/10.1016/j.eti.2024.103667.

Marlinda, A.R., Thien, G.S.H., Shahid, M., Ling, T.Y., Hashem, A., Chan, K.Y., Johan, M. R., 2023. Graphene as a lubricant additive for reducing friction and wear in its liquid-based form. Lubricants 11, 29. https://doi.org/10.3390/lubricants11010029.

Miller, G.P., Kintigh, J., Kim, E., Weck, P.F., Berber, S., Tománek, D., 1998. Hydrogenation of single-wall carbon nanotubes using polyamine reagents: combined experimental and theoretical study. J. Am. Chem. Soc. 130, 2296–2303. https://doi.org/10.1021/ja0775366.

Mohan, V.B., Jayaraman, K., Bhattacharyya, D., 2020. Brunauer–Emmett–Teller (BET) specific surface area analysis of different graphene materials: a comparison to their structural regularity and electrical properties. Solid State Commun. 320, 114004. https://doi.org/10.1016/j.ssc.2020.114004.

Molenda, J., Dziosa, K., Makowska, M., Łożyńska, M., Kozdrach, R., Radulski, P., Hodniczek, T., Musioł, F., 2025a. Effect of microstructure and biochar additive content on the rheological properties of grease. Przemys. ł Chem. 104 (10), 986–991. https://doi.org/10.15199/62.2025.10.4.

Molenda, J., Makowska, M., Kubacki, J., Sikora, M., Łuszcz, M., Osuch-Słomka, E., 2025b. Investigation of the chemical structure and antiwear performance of biochar used as a grease additive. Wear 576-577, 206143. https://doi.org/10.1016/j.wear.2025.206143.

Morstein, C.E., Dienwebel, M., 2021. Graphite lubrication mechanisms under high mechanical load. Wear 477, 203794. https://doi.org/10.1016/j.wear.2021.203794.

Naboka, O., Yim, C.H., Abu-Lebdeh, Y., 2021. Practical approach to enhance compatibility in silicon/graphite composites to enable high-capacity Li-Ion battery anodes. ACS Omega 6, 2644–2654. https://doi.org/10.1021/acsomega.0c04811.

Nandiyanto, A.B.D., Oktiani, R., Ragadhita, R., 2019. How to read and interpret FTIR Spectroscope of Organic Material. Indones. J. Sci. Technol. 4, 97–118. https://doi.org/10.17509/ijost.v4i1.15806.

Nazari, S., Rahimi, G., Nezhad, A.K.J., 2019. Effectiveness of native and citric acid-enriched biochar of Chickpea straw in Cd and Pb sorption in an acidic soil. J. Environ. Chem. Eng. 7, 103064. https://doi.org/10.1016/j.jece.2019.103064.

Ostyn, N.R., Thijs, B., Steele, J.A., Sree, S.P., Wangermez, W., Teyssandier, J., Minjauw, M.M., Li, J., Detavernier, C., Roeffaers, M.B.J., De Feyter, S., Martens, J.A., 2021. Controlled graphite surface functionalization using contact and remote photocatalytic oxidation. Carbon 172, 637–646. https://doi.org/10.1016/j.carbon.2020.10.069.

Özsin, G., Kılıç, M., Apaydın-Varol, E., Pütün, A.E., 2019. Chemically activated carbon production from agricultural waste of chickpea and its application for heavy metal adsorption: equilibrium, kinetic, and thermodynamic studies. Appl. Water Sci. 9, 56. https://doi.org/10.1007/s13201-019-0942-8.

Patel, M.R., Panwar, N.L., 2023. Biochar from agricultural crop residues: environmental, production, and life cycle assessment overview. Resour. Conserv. Recycl. Adv. 19, 200173. https://doi.org/10.1016/j.rcradv.2023.200173.

Rahman, M.M., Islam, M., Roy, R., Younis, H., Ainahyan, M., Younes, H., 2022. Carbon nanomaterial-based lubricants: review of recent developments. Lubricants 10 (11), 281. https://doi.org/10.3390/lubricants10110281.

Regulation of the European Parliament and of the Council establishing a framework for ensuring a secure and sustainable supply of critical raw materials and amending regulations (EU) no 168/2013, (EU) 2018/858, (EU) 2018/1724 and (EU) 2019/1020. European Parliament and of the Council EU, 2024.

Reich, S., Thomsen, C., 2004. Raman spectroscopy of graphite. Philos. Trans. A Math. Phys. Eng. Sci. 362, 2271–2288. https://doi.org/10.1098/rsta.2004.1454.

Shell, 2025. 3 simple steps for effective f ifth wheel greasing while in transit. Technical Report.

Sieradzka, M., Kirczuk, C., Kalemba-Rec, I., Mlonka-Mędrala, A., Magdziarz, A., 2022. Pyrolysis of biomass wastes into carbon materials. Energies 15, 1941. https://doi.org/10.3390/en15051941.

Song, H., Wang, Z., Yang, J., 2016. Tribological properties of graphene oxide and carbon spheres as lubricating additives. Appl. Phys. A 122, 933. https://doi.org/10.1007/s00339-016-0469-x.

Srinivasan, P., Sarmah, A.K., 2015. Characterisation of agricultural waste-derived biochars and their sorption potential for sulfamethoxazole in pasture soil: a spectroscopic investigation. Sci. Total Environ. 502, 471–480. https://doi.org/10.1016/j.scitotenv.2014.09.048.

Tamashausky, A., 2002. The effect of graphite type, purity and concentration on the performance of a clay filled polyalphaolefin grease, based on four ball wear (ASTM D2266) with Coefficient of Friction and Load Wear Index (ASTM D2596). Spokesman 12, 10–25.

Tan, H., Guo, Y., Wang, D., Cui, Y., 2022. The development of a Cu@Graphite solid lubricant with excellent anti-friction and wear resistant performances in dry condition. Wear 488489, 204181. https://doi.org/10.1016/j.wear.2021.204181.

Thommes, M., Kaneko, K., Neimark, A.V., Olivier, J.P., Rodriguez-Reinoso, F., Rouquerol, J., Sing, K.S.W., 2015. Physisorption of gases, with special reference to the evaluation of surface area and pore size distribution (IUPAC Technical Report). Pure Appl. Chem. 87, 1051–1069. https://doi.org/10.1515/pac-2014-1117.

Ţucureanu, V., Matei, A., Avram, A.M., 2016. FTIR spectroscopy for carbon family study. Crit. Rev. Anal. Chem. 46, 502–520. https://doi.org/10.1080/10408347.2016.1157013.

Vaghela, D.R., Pawar, A., Sharma, D., 2023. Effectiveness of wheat straw biochar in aqueous Zn removal: correlation with biochar characteristics and optimization of process parameters. Bioenerg. Res. 16, 457–471. https://doi.org/10.1007/s12155-022-10471-9.

Vazirisereshk, M.R., Martini, A., Strubbe, D.A., Baykara, M.Z., 2019. Solid Lubrication with MoS2: a review. Lubricants 7, 57. https://doi.org/10.3390/lubricants7070057.

Vidoeski, B.A., Jovanović, S.P., Holclajtner-Antunović, I.D., Bajuk-Bogdanović, D.V., Budimir, M.D., Marković, Z.M., B. Todorović Marković, B.M., 2016. Raman study of the interactions between highly ordered pyrolytic graphite (HOPG) and polyoxometalates: the effects of acid concentration. J. Serb. Chem. Soc. 81, 777–787. https://doi.org/10.2298/JSC160301055V.

Wakchaure, M.B., Menezes, P.L., 2025. Advances in the tribological performance of graphene oxide and its composites. Materials 18 (15), 3587. https://doi.org/10.3390/ma18153587.

Wang, N., Hu, J., Li, J., Tan, Z., Dong, L., Mei, N., Wang, H., 2022. Structural properties and reactivity variations of wheat straw char catalysts in volatile reforming. Green. Process. Synth. 11, 1052–1063. https://doi.org/10.1515/gps-2022-0084.

Wijitkosum, S., Jiwnok, P., 2019. Elemental composition of biochar obtained from agricultural waste for soil amendment and carbon sequestration. Appl. Sci. 9, 3980. https://doi.org/10.3390/app9193980.

Wu, S., Tian, S., Menezes, P.L., Xiong, G., 2020. Carbon solid lubricants: role of different dimensions. Int J. Adv. Manuf. Technol. 107, 3875–3895. https://doi.org/10.1007/s00170-020-05297-8.

Wystalska, K., Kwarciak-Kozłowska, A., 2021. The effect of biodegradable waste pyrolysis temperatures on selected biochar properties. Materials 14, 1644. https://doi.org/10.3390/ma14071644.

Yu, H., Chen, H., Zheng, Z., Qiao, D., Feng, D., Gong, Z., Dong, G., 2023. Effect of functional groups on tribological properties of lubricants and mechanism investigation. Friction 11, 911–926. https://doi.org/10.1007/s40544-022-0630-9.

Zhang, X., Luster, B., Church, A., Muratore, C., Voevodin, A.A., Kohli, P., Aouadi, S., Talapatra, S., 2009. Carbon nanotube−MoS2 composites as solid lubricants. ACS Appl. Mater. Interfaces 1, 735–739. https://doi.org/10.3390/lubricants12090308.

Zhang, J., Zhang, X., Wang, C., Sun, H., Zhou, S., 2022. Optimal nitrogen fertilizer, which determines straw properties, and pyrolysis temperatures produce desired-biochars that can be used as a soil amendment. Chemosphere 308, 136572. https://doi.org/10.1016/j.chemosphere.2022.136572.

Zhao, L., Cao, X., Mašek, O., Zimmerman, A., 2013. Heterogeneity of biochar properties as a function of feedstock sources and production temperatures. J. Hazard. Mater. 256–257, 1–9. https://doi.org/10.1016/j.jhazmat.2013.04.015.

Ziętara, W., Zieliński, M., 2018. Straw as alternative energy source or organic matter in the soil. Zagadnienia Ekon. Rolnej 355, 28–40. https://doi.org/10.30858/zer/92060.